Bedding attitudes as a sequence stratigraphy proxy : A case study from borehole images, Integrated Ocean Drilling Program Leg 313, Hole M28

Christophe Basile, D. Monteverde

Geosphere; April 2014; v. 10; no. 2; p. 207–220; doi:10.1130/GES00856.1
Results of IODP Exp313: The History and Impact of Sea Level Change Offshore New Jersey themed issue

Bedding attitudes as a sequence stratigraphy proxy : A case study from borehole images, Integrated Ocean Drilling Program Leg 313, Hole M28

C. Basile [(1)], D. Monteverde [(2)]

Adresses
(1) : ISTerre, Université Joseph Fourier, Grenoble, France. Corresponding author : cbasile@ujf-grenoble.fr
(2) : Department of Earth and Planetary Sciences, Rutgers University, Piscataway, NJ 08854.

Abstract
In this study we investigate the relationship between the dips of seismic reflectors, which are used to define sequence boundaries, and the orientation (dip and dip direction) of bedding surfaces at core scales. Sequence boundaries from seismic data and lithostratigraphic boundaries from cores and logs are compared with the bedding orientations measured on borehole images of Miocene siliciclastic sediments at Integrated Ocean Drilling Program Expedition 313 Site M28. It is not surprising that bedding orientations show huge variations at scales that are too small to be detected on seismic profiles. However, changes of orientation defined as rotation between two successive intervals match the depths of approximately half of the seismic sequence boundaries. While they do not match boundaries between lithostratigraphic units, changes of orientation frequently correlate with maxima and minima in the gamma ray signal, suggesting that they are related to changes in depositional processes rather than to changes in lithology. This study suggests for the first time that bedding attitudes can be used as a stratigraphic tool at various scales from bed to bed across depth intervals of tens of meters.

Keywords
sequence stratigraphy; dipmeter; correlations

INTRODUCTION

As initially developed by Vail et al. (1977), sequence stratigraphy was based on the interpretation of the geometric relationships between seismic reflectors imaged in seismic data. Stratigraphic units can be described as sets of concordant seismic reflectors with slight and progressive internal changes of dip that are bounded by surfaces (onlaps, toplaps, downlaps, truncations) where sudden changes of dip occur. Sequence boundaries and maximum flooding surfaces are identified from those changes (Fig. 1). Seismic profiles are adequate for investigating geometries within sedimentary basins at horizontal scales that range from 1 to hundred of kilometers; however their vertical resolution in basin studies is rather poor, frequently from 10 to 50 meters in depth, resulting in poor age resolution (frequently a few million years).

Many seismic sequence interpretations at continental margins incorporate drill core and outcrop studies, both offshore and onshore, to achieve better vertical resolution than can be expected from seismic data alone (e.g. van Wagoner et al., 1990; Greenlee et al., 1992; Bellotti et al., 1994). Wells drilled in sand-rich continental margins typically have poor core recovery and to compensate analyses often rely on continuous recordings from geophysical downhole logs to fill the data gaps. For example, the U.S. Geological Survey Atlantic Margin Coring Project (AMCOR, Hathaway et al., 1976) averaged only 27% recovery over 20 sites on the U.S. Mid-Atlantic continental shelf, but collected downhole logs to measure properties of the entire sedimentary section of each well. Exact vertical placement of incompletely recovered cores proved elusive without the log data. Borehole images, another part of the suite of modern log tools, have proved extremely effective in identifying core placement and orientation (MacLeod et al., 1994; Haggas et al., 2001; Inwood et al., 2008), determining facies and paleoflow direction in both siliciclastic and carbonate rocks (Luthi and Banavar, 1988; Luthi, 1990; Prensky, 1999; Donsellar and Schmidt, 2005, 2010; Luthi et al., 2006; Puga-Bernabéu and Betzler, 2008), identifying unconformities (Prosser et al., 1999) and leading to structural analysis for formation assessment and permeability studies involving both petroleum and groundwater (Prensky, 1999; Parkinson et al., 1999; Williams

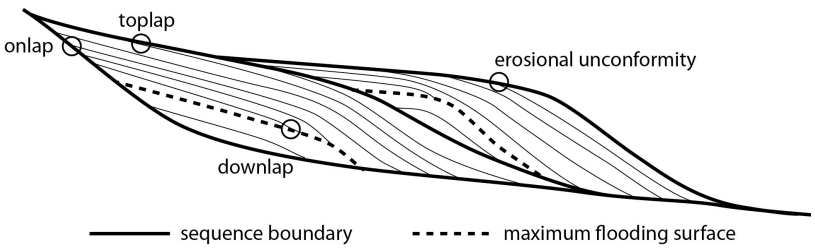

Figure 1: Schematic stratigraphic sequences and the angular relationships defining the boundaries of stratigraphic units. No scale; vertical exaggeration is very great.

and Johnson, 2004; Yamada et al., 2011).

Integrated Ocean Drilling Program Expedition 313 (IODP Exp 313) was sited along the New Jersey margin (Fig. 2) to test the sequence stratigraphic model using coreholes that sampled individual sequences at several different locations of clinoform geometry imaged by high-resolution seismic data (Mountain et al., 2010). At these drill sites, lithostratigraphy can be used to infer changes in sedimentary environment, and suggest paleo-depths, which can be compared with predictions from seismic profile analysis. Leg 313 data also include acoustic images of the borehole wall in limited intervals. From these images one can measure dip and dip direction as intersected by the borehole. The purpose of the work reported here is to investigate if and how the changes in orientation observed in core and borehole images can be used as a stratigraphic tool for units whose thicknesses ranging in thickness from centimeters (strata scale) to tens of meters (seismic profile scale). The work described in this report attempts to use bedding attitudes as sampled in borehole images to define and correlate sedimentary sequence boundaries between seismic and core scales.

INVESTIGATED SITE

Location

IODP Leg 313 drilled three sites, M27, M28 and M29, on the continental shelf offshore New Jersey in water depths of < 40 m (Fig. 2). These sites were located to sample topsets, foresets and toesets of several Miocene clinoform structures (Expedition 313 Scientists, 2010a). Acoustic borehole images were acquired at the three sites, but the limited number of sedimentary beds identified on images from Sites M27 and M29 did not allow any conclusive interpretation. In this study, we present the observations and interpretations from acoustic borehole images at Site M28, where sufficient data density and quality are available from 396 to 656 meters below seafloor (mbsf).

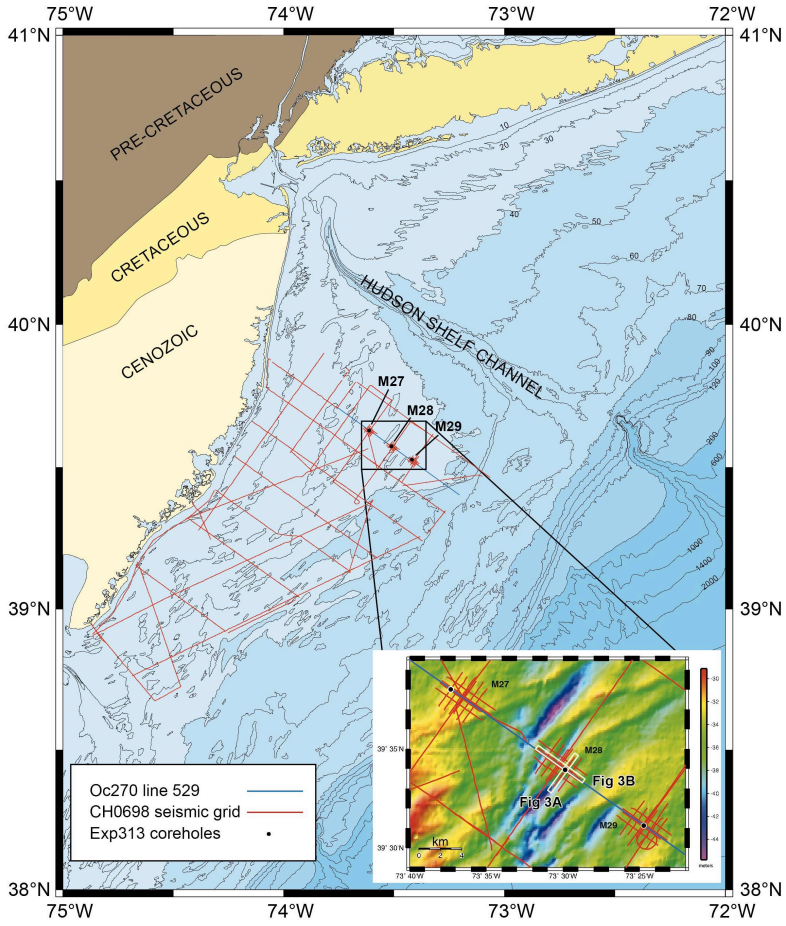

Figure 2: Location of the Integrated Ocean Drilling Program Expedition 313 (Exp313), Site M28 studied drillhole offshore New Jersey (modified from Expedition 313 Scientists, 2010c). Oc270-R/V Oceanus; CH0698-R/ Cape Hatteras.

Seismic Stratigraphy

Several generations of seismic data of increasing resolution have imaged the progradational and aggradational clinoformal structures that document the Neogene growth of the New Jersey region of the US Mid-Atlantic margin (Greenlee and Moore, 1988; Greenlee et al., 1992; Mountain et al., 1994; Fulthorpe et al., 1996; Steckler et al., 1999). In 1995 High-resolution multichannel seismic data (~5 m resolution) were collected; the R/V *Oceanus* (line Oc270) targeted the outer shelf and slope but also ran a dip line across the continental shelf in preparation for Expedition 313. Similar seismic equipment aboard the R/V *Cape Hatteras* (CH0698) in 1998 imaged the inner continental shelf and sampled a dense hazard grid surrounding the proposed location of each Exp 313 corehole. Several candidate sequence boundaries (Monteverde et al., 2008) traced in the CH0698 seismic data and Oc270 line 529 were targeted in Exp 313 (Fig. 3). These seismic surfaces defined boundaries of individual seismic sequences, named by the basal seismic reflector that the Exp 313 corehole transect sampled. Site M28 penetrated seismic surfaces m5.32, located only a few meters above the studied interval, and m5.33, m5.34, m5.35, m5.4, m5.45, m5.47, m5.6, m5.7 and m5.8 that were all recorded by the borehole imager (Fig. 3 and Table 1) (Expedition 313 Scientists, 2010c). The clinoform rollover positions are located northwest or updip of Site M28 for all these surfaces, therefore no topset

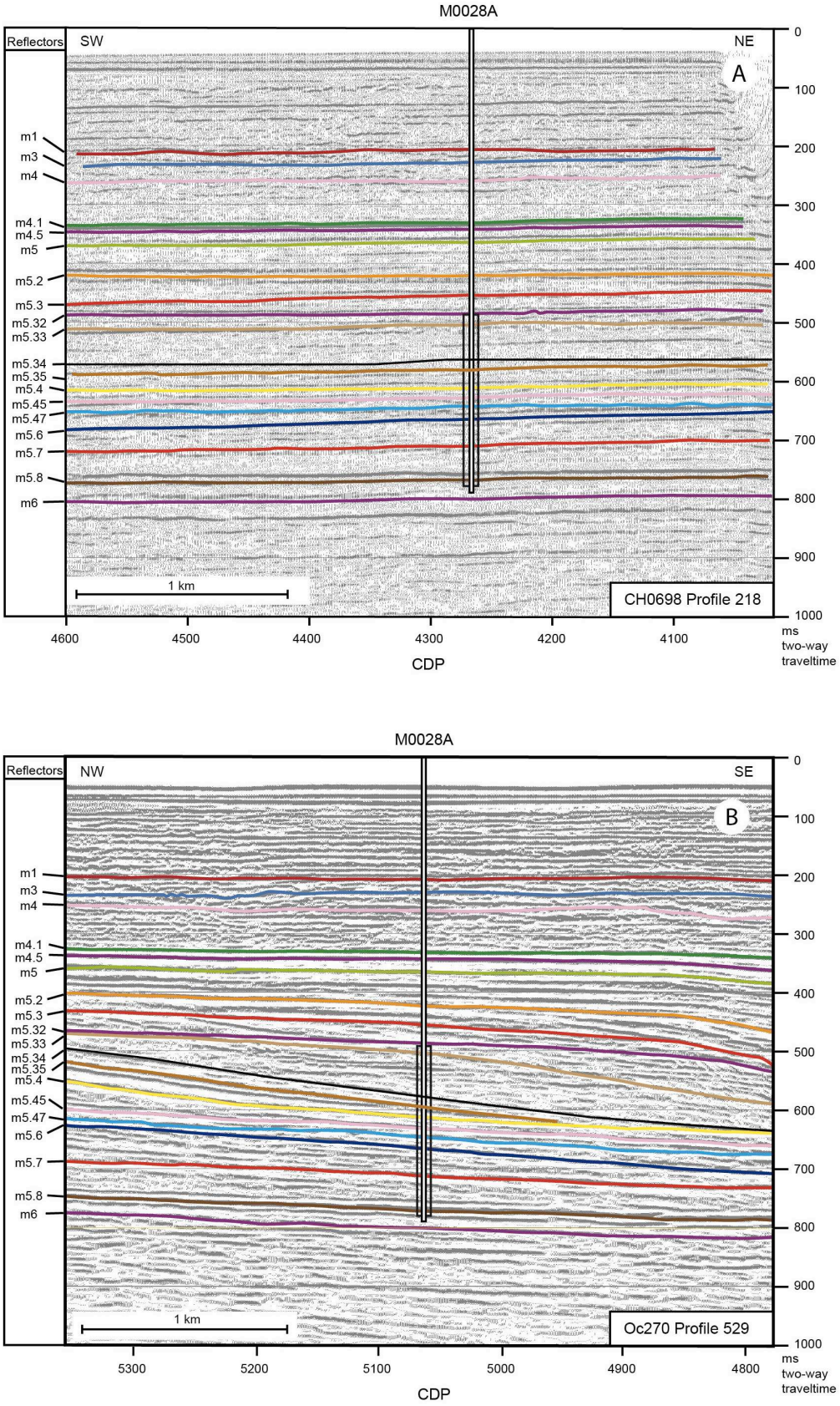

Figure 3: Two perpendicular seismic lines across Integrated Ocean Drilling Program Expedition 313 Site M28 (location in Fig. 2). The vertical boxes on the seismic lines indicate the studied interval. Vertical exaggeration is 3.35 for 2 km/s seismic velocity. CDP: Common Depth Point. Modified from Expedition 313 Scientists (2010c). Oc270-R/V Oceanus; CH0698-R/ Cape Hatteras.

seismic surfaces	depth (ms)	depth (mbsf)	dip direction	dip (ms/km)	dip (°)	remarks (Expedition 313 Scientists, 2010b)
m5.3	458	363				
m5.32	488	391	N148°	9	0.6	
m5.33	506	415	N136°	26	1.7	downlap on m5.4
m5.34	562	475	N135°	46	2.8	
m5.35	580	495	N136°	41	1.7	
m5.4	612	512.33	N139°	21	1.1	onlap and downlap surface
m5.45	633	533.59	N150°	18	1	
m5.47	646	545.5	N138°	22	1.3	toplap surface, incised
m5.6	666	567.5	N146°	24	1.4	toplap surface
m5.7	710	611.6	N155°	15	0.8	downlap surface
m5.8	772	662.98	N149°	11	0.6	

Table 1: Characteristics of the seismic surfaces in the studied interval. Dip and dip direction are computed assuming a planar shape of the surfaces in a 1 km-diameter circle centered on Integrated Ocean Drilling Program Site 28. The depths measured on seismic lines are in two-way traveltime below sea level (mbsf-meters below seafloor).

geometries were analyzed in the borehole images at site M28 (Expedition 313 Scientists, 2010c). Surfaces m5.33 to m5.4 represent progradational foresets, while the underlying surfaces represent toesets dominated by aggradation (Fig. 3). Northwest of Site M28 the highly irregular reflector m5.47 overlies a series of toplap surfaces and has been related to erosion (Monteverde et al., 2008).

Seismic surfaces on perpendicular seismic lines offer the opportunity to calculate their true dip and dip direction. The mean dip direction trends N145°, with only slight variations from N135° for the foresets (m5.33 to m5.35) to N155° (Table 1). The mean dip is only 1°, far from the steep slopes observed on the seismic lines displayed with huge vertical exaggeration. Dips vary from 0.6° for the topset (m5.32) and bottomset (m5.8) surfaces to 2.8° for m5.34 representing a foreset within the thickest deposition seaward of the clinoform rollover.

Lithostratigraphy

Lithostratigraphy of the sediments we analyzed is based on the descriptions of split cores by the Exp 313 sedimentologists (Expedition 313 Scientists, 2010c.) The overall lithology is siliciclastic, with grain sizes varying in the studied interval from coarse sand at the top to silty clay at the bottom. Several intervals contain large concentrations of glauconite, locally as much as 80%. All lithologies within the M28 studied interval were grouped into four units (III-VI), with units III and V further subdivided into subunits (IIIB-IIID and VA-VC) (Expedition 313 Scientists, 2010c, Fig. 7). Expedition 313 sedimentologists concluded that these sediments were deposited on a wave-dominated marine shelf, close to a fluvial source, based on the abundance of detrital micas and organic matter (Expedition 313 Scientists, 2010c). Deposition varied from shoreface (subunit IIIB) to deeper environments: shoreface-offshore transition to offshore (subunits IIIC and IIID), toe of slope apron (subunit IIID, units IV and V), and offshore (unit VI) (Fig. 7).

Laminations observed in cores are mainly parallel, and frequently subhorizontal. However, some intervals display inclined sedimentary bedding, especially in subunit IIIC and unit V, where apparent dips in core sections reach 15 to 20°.

Gamma Ray Logging

Coring does not provide complete coverage of the drilled section even with an elevated recovery (80% at Site 28). Downhole logging data, such as gamma ray measurements, however, provide continuous information, and aid the reconstruction of the entire section drilled (Fig. 7). After Exp 313 cores were collected, but before they were split, gamma ray data were also recorded directly on the cores, thereby providing a clear, unequivocal tie to the downhole measurements and reducing discrepancies between core and logging depths particularly in intervals of poor core recovery. The available gamma ray logs include spectral analysis that provides K, U and Th contents of the buried sediments to be identified, further characterizing the penetrated sediments (Expedition 313 Scientists, 2010b).

METHODS

Borehole Images

Several sets of borehole images were recorded in Hole M28 using the acoustic borehole televiewer ALT ABI40 (Expedition 313 Scientists, 2010b). Acoustic impedance images provide information on the reflectivity of the borehole wall, while travel time images record the diameter and shape of the borehole. Both images are mainly controlled by the lithology. Lithologic variability appears as a reflectivity change in the borehole images, and frequently as a hole diameter change (Fig. 4). In the unlithified sediments, the coarser layers, typically medium to coarse sands, appear as less reflective and are associated with an enlarged borehole.

The resolution of the borehole televiewer image is mainly controlled by the speed at which the logging tool is drawn up the borehole. In Hole M28, high horizontal resolution (288 pixels, i.e. approximately 1 mm/pixel for the 96 mm bit size) was acquired only between 396 and 426 mbsf, and low resolution (72 pixels, 4 mm/pixel) was obtained in the lower section (426-656 mbsf). Vertical resolution also varies with the tool speed, from 2 mm/pixel at high resolution to 4 mm/pixel at low resolution.

Borehole images are displayed as an unrolled cylinder, with the orientation (0° to 360° from north to north; magnetic north inside the borehole is recorded with every borehole image) given on the x-axis (Fig. 4). In this representation, a dipping plane that crosses the borehole appears as a sinusoid. The orientation of the lower point of the sinusoid is the dip direction, and the dip is deduced from the amplitude of the sinusoid and hole diameter (Serra, 1989). Dip can vary from a high-amplitude sinusoid defining a steeply dipping feature to a horizontal line corresponding to one that is horizontal. Dip and dip direction are computed in the borehole reference frame so the geographic and vertical orientation of the borehole are important pieces of information. Hole M28 deviates <1° from vertical so the borehole reference frame is assumed equivalent to the geographic frame, and no corrections were applied for hole deviation. Given the poor resolution of the borehole images, the uncertainty on dip and dip direction measurements is several degrees and >10°, respectively. Moreover, poor image resolution severely complicates the determination if horizontal or subhorizontal changes recorded in the images actually relate to artifacts commonly produced by changes in the speed the logging tool was raised up the borehole. As a consequence, these subhorizontal surfaces were frequently not measured, resulting in a probable underestimation of low-dipping surfaces.

Comparison Between Cores and Borehole Images

Comparison between cores and borehole images increases the confidence in both the position and accuracy of the measurements performed on images. However, several problems can make this comparison difficult.

The first problem relates to the core orientation. The borehole is observed as an unrolled cylinder, providing true orientations (dips and dip directions). Cores are cut on vertical sections that are not oriented on purpose, i.e. not parallel to the dip direction. Consequently, the dips observed on core sections are apparent dips that underestimate true dips. The worst case is a core cut perpendicular to the dip direction, where steeply-dipping strata appear horizontal on the planar cut section.

The second problem arises from the absence of core orientation in a geographic frame, making it impossible to measure dip direction based on cores alone.

The different depth

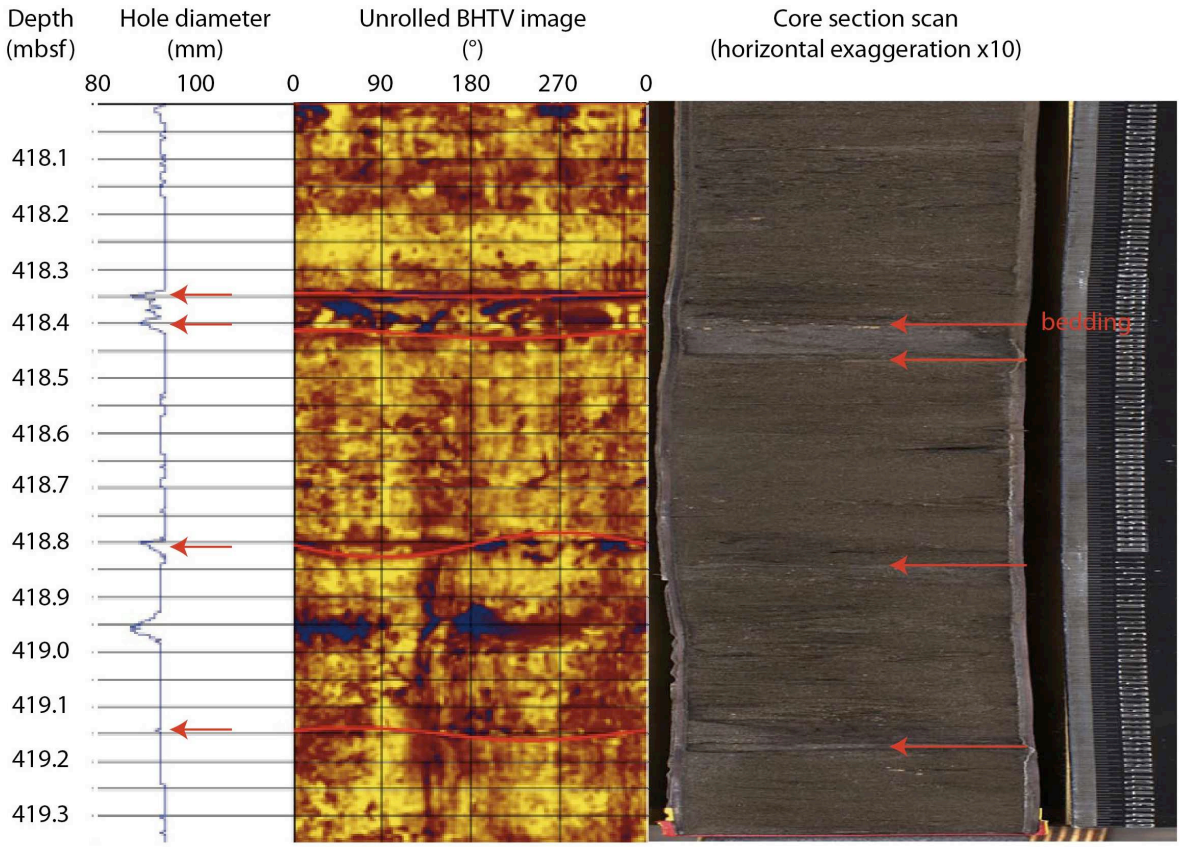

Figure 4: Example of correlation of borehole image (acoustic impedance) and core section (Hole M28, Core 80, Section 2; mbsf-meters below seafloor). Beds are underlined by red sinusoids on borehole televiewer (BHTV) images, by red arrows on the core section (horizontal exaggeration 10) and on the hole diameter curve. In this example, caliper and BHTV depths are systematically 8 cm shallower than depths to corresponding features in the core (see the text).

measurements between cores and log data need to be resolved (Fig. 4). Core depths are linked to the pipe length, while logging depths are linked to the wireline length, introducing the possibility of small (<1 m) discrepancies between the two. Moreover, when core length is shorter than the drilled interval (i.e. when recovery is <100%), the recovered core is not precisely located in the drilled interval, adding uncertainty (less than the 3 m drilled interval) to the depth correlation unless additional information such as borehole gamma logs and core gamma data can be correlated.

TrackDip Processing Method

Systematic measurement of bedding attitudes provides a large amount of data that can be difficult to interpret. As an example, global representations such as rose diagrams, dip histograms or stereographic plots provide a global view of the orientation of the strata in the studied interval, but do not delineate the bedding variations with depths. However, the three-dimensional changes of orientation are not easy to measure from plots of dip and dip direction with depth (either independently or as tadpole plots). We used the TrackDip processing method (Basile et al., 2009) to identify the most important changes in orientation, their depths and characteristic scales.

TrackDip is based on a multi-scalar approach, searching for the changes in orientation at all scales from the entire studied interval to the thinnest interval between two measurements (centimeters), with a $10^{0.1}$ ratio between consecutive scales (i.e. 10 investigated scales for 1 to 10 m thick intervals). For each interval, a mean orientation is computed. Then the mean orientation of successive intervals is compared and any change in attitude defined by a change in rotation axes, rotation angles and/or rotation ways between adjacent intervals. Calculation of the rotation way involves defining the azimuth of the lower plane after rotating both the upper and lower planes until the upper plane is horizontal (Basile et al., 2009). For a given depth, scattered orientations result in large variations of mean orientation as the interval scale changes, but dominant changes still can be tracked through the scale changes. Consequently, there is more confidence in the orientation tracked over a large number of scales, i.e. large number of measurements, than for a small number of scales. Three successive scales are considered arbitrarily as a minimum, implying at least four measurements at the larger scale to ensure that the mean orientations change from one scale to another. Furthermore, in Basile et al. (2009) it was shown that considering only the orientation changes tracked from window sizes containing more than seven measurements can be a useful cut-off to eliminate the effects of random changes of ± 4° for dip and ± 15° for the dip direction. For each measurement, the window size containing seven measurements is the depth difference between the three downward and the three upward measurements.

We first present this method in the following theoretical case (Fig. 5), similar to what can be expected from the changes of orientation that can be seen on seismic lines. We applied TrackDip processing to a synthetic data set that contain 40 measurements randomly distributed by depth in a 40 m-thick section. In this simple case, a single orientation change occurs between 0-40 m at a depth of 15 m with beds oriented 3/135 (dip/dip direction) above and 1/150 below the change (red symbols in Figs. 5A, 5B). This orientation change mimics what can be expected from the seismic profile crossing Site M28 (Fig. 3; Table 1); it represents a 2.05° rotation around a N38° trending rotation axis. From this simple initial setting, a more muddled case was created by introducing a random orientation change of ± 4° in dip and ±4°/sin(dip) in azimuth at each data depth (black symbols in Figs. 5A, 5B). The resulting mean orientations are 2.5/125.6 and 0.3/169.6 in the upper and lower intervals, respectively, and correspond to a 2.29° rotation around a N30.4° trending rotation axis (Fig. 5F). The maximum rotation observed between two consecutive scattered measurements is 7.32°.

TrackDip provides an objective and rigorous comparison of the mean orientation of bedding surfaces between adjacent intervals. For example, at 16.6 m depth and a 6.34 m scale in our hypothetical example, the tilt between the two 6.34-m-thick intervals (from 10.26 to 22.94 m) is characterized by N33° trending axis, N303° rotation way (dip direction for the lower interval when the upper one is set to horizontal), and 3.83° tilt angle (Fig. 6). At a smaller scale (5.04 m), a similar rotation can be found in the same depth interval: N12° axis, N282° rotation way, 3.24° tilt at 14.73 m (Fig. 6). In this example, we consider only rotation angles >3°, and rotations are considered to be similar when the variations for the trends of the rotation axis and rotation way are <±30°. In Figure 6, the arrows indicate the rotations that can be tracked at various scales, using the >3° and ±30° cut-offs for rotation angle and trends, respectively. Gray arrows indicate rotations that cannot be tracked over three or more successive scales with changing tilt parameters.

In the test example, using this additional cut-off restrains the tracked rotations to the only one highlighted in red in Figure 6 and shown in Figure 5C. For this selected rotation, the window size where the rotation angle reaches a maximum is assumed to correspond to the most representative (or the least noisy) signal. This best rotation is identified for a 4-m thick window size at 15.77 depth; it's a 3.85° rotation around a N39° trending

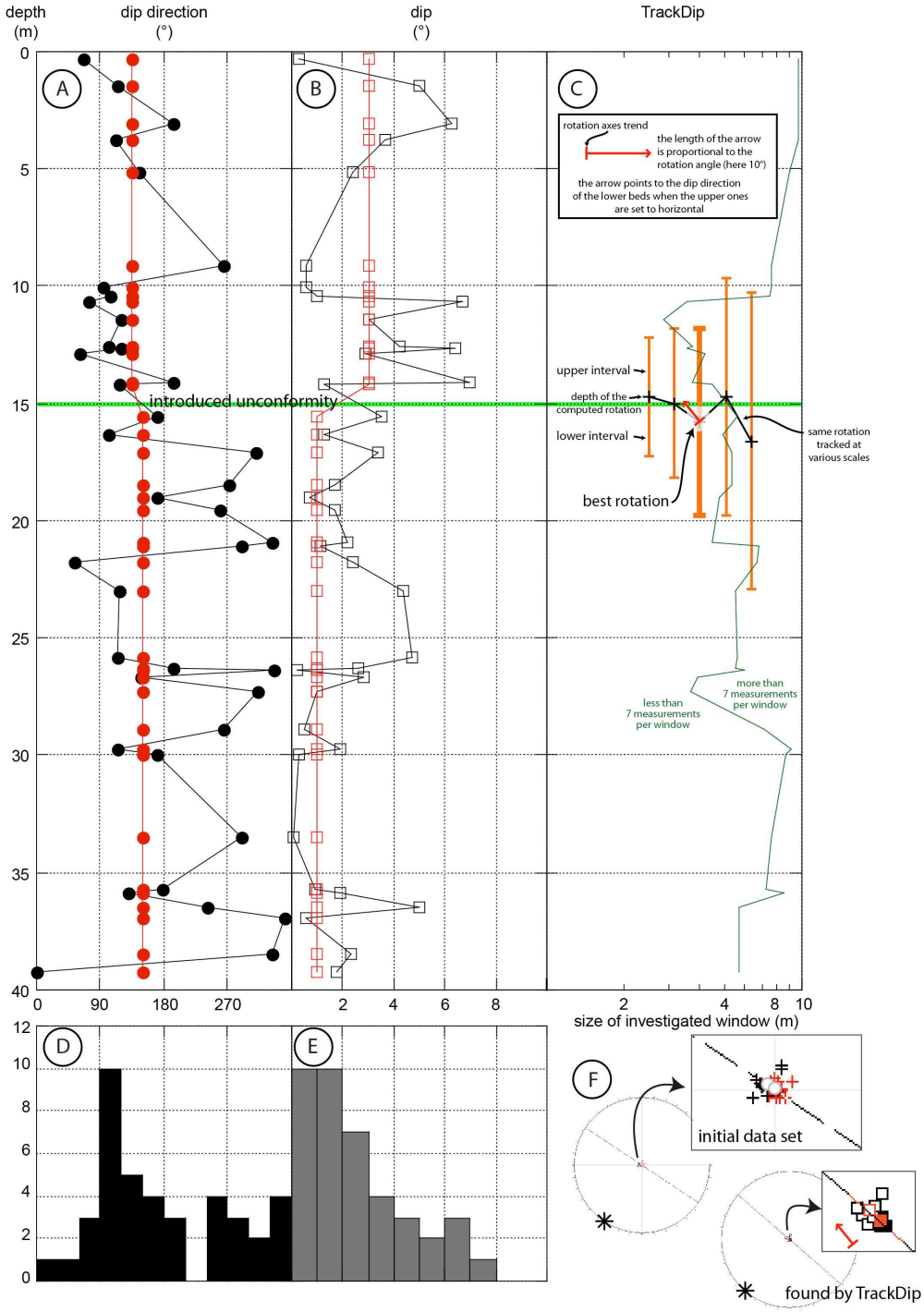

Figure 5: Display of bedding attitudes and TrackDip (Basile et al., 2009) processing for a synthetic data set with a 2° unconformity located at 15 m (horizontal green line) (see text for comments). (A) Variation of dip direction with depth. Red dots indicate the initially fixed dip directions, black dots are the scattered ones. (B) Dips of the initial (red boxes) and scattered (black boxes) beds. (C) Display of TrackDip results (for details, see Fig. 6 and text). The green line indicates the depth interval that contains seven measurements (for each measurement, from the third measurement downward to the third upward). (D) Azimuth histogram of scattered data (same horizontal scale as A). (E) Dip histogram of scattered data (same horizontal scale as B). (F) Stereonet plots (Wulf canvas, lower hemisphere) of the bedding data set. On the left side, the stereonet shows all data: black crosses are from the upper interval (0-15 m), red crosses from the lower one (15-40 m). Circles indicate the mean values for both intervals. The great circle (dashed line) and associated pole (star is rotation axis) are calculated from the mean values. On the right side, the stereonet shows the measurements for the rotation identified by TrackDip: open black boxes are data from the upper interval, filled black boxes from the lower interval; the same red symbols are the mean values for each interval, and the rotation is computed from the mean value.

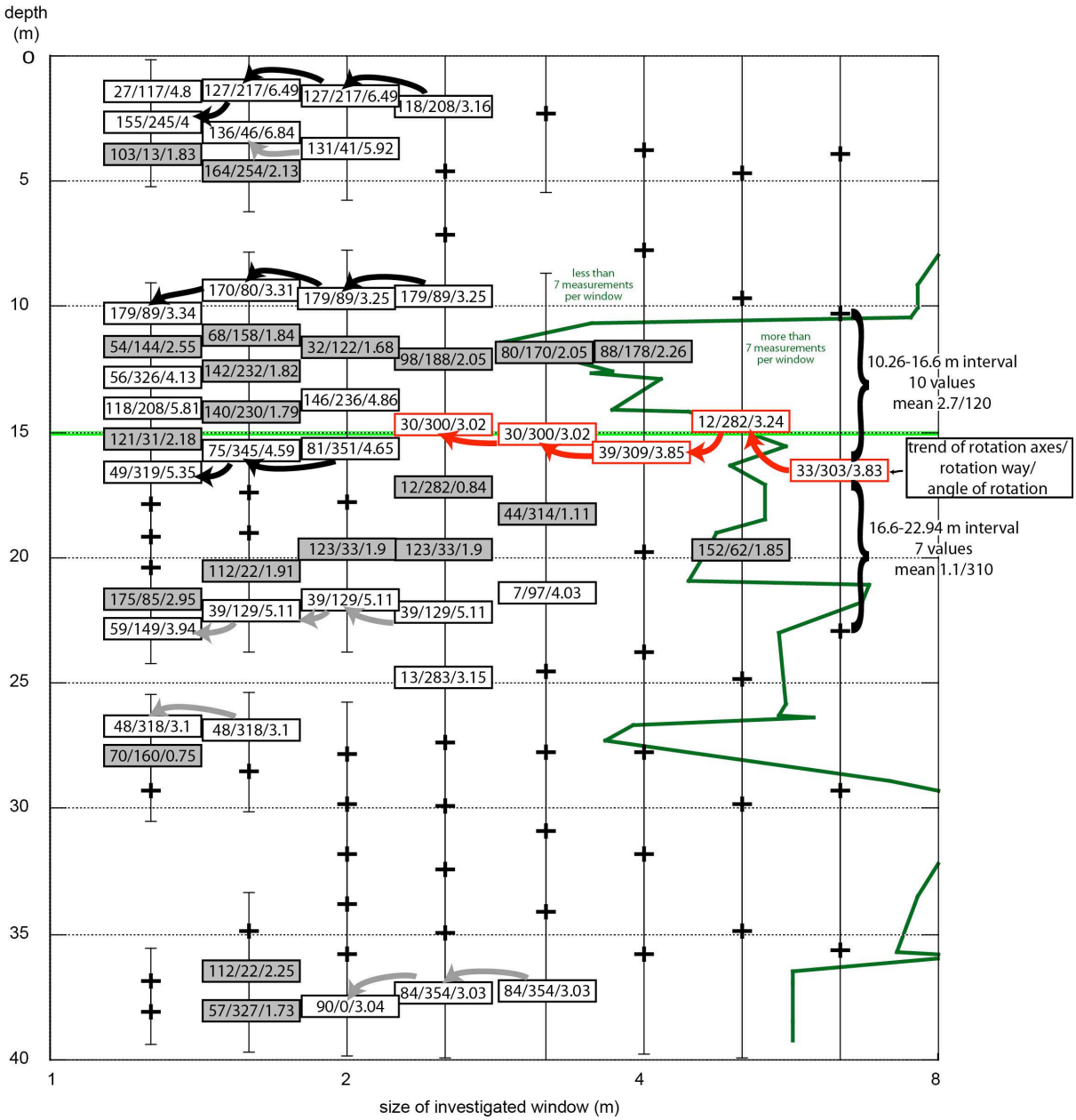

Figure 6: Detailed TrackDip (Basile et al., 2009) processing for the test example presented in Figure 5 (see also the text for comments). Each cross or box represents the depth and window size where a rotation is computed between the upward and downward intervals (thin vertical lines from cross to cross). Boxes contain the trend of the rotation axes, the rotation way (dip direction in the lower interval when the upper one is set to horizontal), and the rotation angle (e.g. 155/245/4). Crosses and shaded boxes are tilts with rotation angle < 3°; all the tilts with higher rotation angle are shown in boxes with a white background. Arrows indicate the rotations that can be tracked for successive window sizes. Gray arrows can be tracked over no more than two window sizes with changing tilt parameters. Red arrows indicate the only tracked rotation that includes a large number of measurements (more than 7 measurements per window, green line); this tracked rotation is also plotted in Figure 5C.

axis (Figs. 6 and 5C). This selected rotation closely matches the expected one: rotation angles and axes are close (3.85° instead of 2.29°, N39° instead of N30°). The identified depth is slightly deeper (15.77 m) than the expected one (15 m).

This test example shows the ability of TrackDip processing to discriminate a very small change in a noisy signal. This is not related to bed-to-bed analysis, but to comparison of sets of beds at decreasing scales, including large scales similar to seismic data resolution. As this method is based on averaged orientations, its accuracy increases with the number and density of bedding orientation measurements.

OBSERVATIONS

Bedding Attitudes

In the upper part (396-426 mbsf) of the studied interval, high-resolution borehole images allow 35 bedding surfaces to be identified and measured (Figs. 7 and 8), including 28 that correlated to strata observed on cores in the deeper part of the interval (Fig. 4). Core recovery was poor in the top 18 m (396-414 mbsf) and dominated by sand in decimeter- to meter-scale thick intervals that lack apparent bedding surfaces (Expedition 313 Scientists, 2010c). Borehole images define 7 bedding surfaces in this poorly recovered interval. Bedding surfaces are more apparent both in core and borehole images from 414 to 426 mbsf, the base of the high-resolution images. Low-resolution borehole images between 426 and 656 mbsf provided 83 additional measurements (Fig. 7) that correlate with lithologic features on available cores. Cores corresponding to the low-resolution images contain either thick sand intervals displaying few well-developed bedding surfaces but locally inclined cross-stratification (typically in the sandy unit V, 525.52–611.28 mbsf), or alternating thin silt and sand layers with clear bedding partings (subunit IIIC from 414.67 to 475.22 mbsf, unit IV from 512.2 to 525.52 mbsf, and unit VI from 611.28 to 662.98 mbsf). All these units were poorly sampled by the borehole images either due to the poor borehole condition in the sandy units, or inadequate image resolution for thin silt and sand beds.

Measurements were not regularly spaced, but preferentially located in the upper part of subunit IIIC, where more than 7 measurements per meter were made between 425 and 427 mbsf (Fig. 7). This spacing is similar to those observed in cores, and probably reflects the sedimentary structure. Below 430 mbsf, image-bedding measurements clearly underestimate the spacing and thickness of individual beds. Only three intervals centered at 470, 550 and 595 mbsf allowed more than 7 measurements per 10 m (Fig. 7). This reduces the opportunity to document orientation changes at small scales to only a few intervals, but does not exclude their existence elsewhere.

Most strata present shallow dips: 42% of all dips are <10° and 72% are <20° (Fig. 7). Some steeply-dipping beds were also observed in borehole images corresponding to those in cores, which are preferentially located in sandy layers. Azimuths (dip direction) are scattered, but some preferential azimuths appear, dominantly N210-240°, and accessory N60-90° (see the histogram at the bottom of the strata azimuth column in Figure 7).

Changes of Orientation

There are two ways to examine the changes of bedding orientation. The first compares each bed with the adjacent beds, both above and below. These bed-to-bed changes make sense if it can be assumed that most of the beds were measured, i.e. only in the interval where high-resolution borehole televiewer (BHTV) was used. The second uses the TrackDip method, which is still valuable even with an incomplete set of measurements (Basile et al., 2009).

Bed-to-Bed Changes in the High-Resolution Interval (396-426 mbsf)

Orientation changes appear to be organized with two preferential rotation axis trends in the interval 406-435 mbsf (Fig. 8). From 435 to 426.6 mbsf, a single N150° rotation axis accounts for all orientation changes. From 426.6 to 423.5 mbsf, the changes of orientation can be fitted by four rotations with similar N55 to N70° horizontal axes, subperpendicular to the downslope direction. From 423.5 to 420.4 mbsf, the change of orientation defines a N170° rotation axis, but comes back to N45° from 420.4 to 419.1 mbsf, and trends N170° from 419.1 to 416.1 mbsf. The measurements between 416.1 and 406 mbsf do not present any meaningful organization.

TrackDip Analysis Including the Low-Resolution Interval (396-656 mbsf)

This analysis only retains rotations >4° as TrackDip methodology has proved effective on synthetic and field dip data characterized by significant rotations >3° (Basile et al., 2009). The selected rotations are tracked from large scales to smaller scales with the same rotation axis and rotation way (± 30°), starting at large scale with more than 7 measurements per window. Identified rotations are labelled from the largest scales to the smallest (1-25, Fig. 7). Each rotation is measured and plotted (red arrows in Figs. 7 and 8) by reference to the underlying interval.

Rotations were identified at various scales controlled by the measurement density estimated from the 7 measurements/window curve (Fig. 7). Where the measurement density is low, only large-scale rotations can be identified, while high measurement density allows us to identify both large-scale and small-scale rotations.

For large scales (>10 m), the upper part (396-510 mbsf) of the studied interval displays N150° to north-south rotation axes, while the lower part (510-656 mbsf) displays perpendicular N70° to N105° rotations axes (Fig. 7). For smaller scales, several rotations observed at bed-to-bed scale can also be identified due to high measurement density (Fig. 8), but most cannot be tracked through several different scales. Some of these rotations (e.g. 20 and 22, 422.6 and 423.8 mbsf; 23 and 25, 425 and 426 mbsf; or 24 and 13, 427.9 and 431.4 mbsf; Fig. 8) can be paired with a similar rotation axis but in an opposite rotation direction which defines horizons of similar bedding attitudes

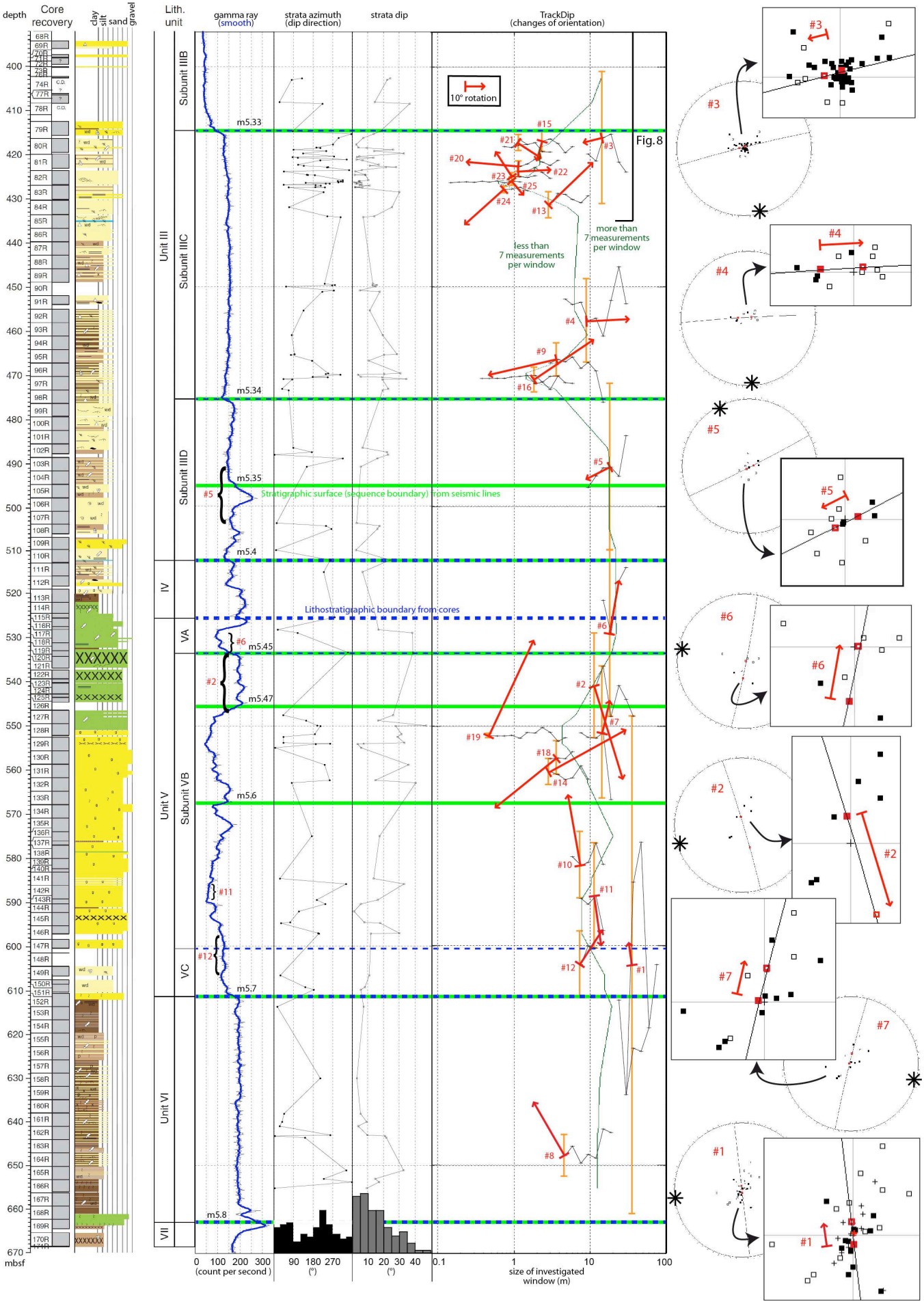
depth
Core recovery
clay
silt
sand
gravel
Lith. unit
gamma ray (smooth)
strata azimuth (dip direction)
strata dip
TrackDip (changes of orientation)
Subunit IIIB
Subunit IIIC
Subunit IIID
Unit III
IV
VA
Subunit VB
Unit V
VC
Unit VI
VII
m5.33
m5.34
m5.35
m5.4
m5.45
m5.47
m5.6
m5.7
m5.8
10° rotation
Fig. 8
less than 7 measurements per window
more than 7 measurements per window
Stratigraphic surface (sequence boundary) from seismic lines
Lithostratigraphic boundary from cores
mbsf
(count per second)
(°)
(°)
size of investigated window (m)

horizon displaying a different trend. These rotations are located in the same interval and are similar in trend to the one determined by the bed-to-bed analysis (Fig. 8). When compared to large scales, small scale changes of orientation present much more variation, even if rotation axes trend more frequently north-south in the upper part and east-west in the lower part.

Correlations

One of the main goals of this work is to determine if changes in bedding attitude in cores and borehole images can be correlated with seismic stratigraphic surfaces. Before IODP Leg 313, several seismic stratigraphic surfaces were defined with seismic profiles of various scales of resolution, all of which pass through the drill sites (Greenlee and Moore, 1988; Greenlee et al., 1992; Steckler et al., 1999; Monteverde et al, 2008). To tie the seismic to the core and/or log data the seismic traveltime must be converted to depth (mbsf). The lithostratigraphy, based on core lithologic descriptions, must be accurately located by ties between downhole natural gamma ray logs and core gamma ray data (Fig. 7).

Significant changes in attitude from one bed to the next at Site M28 (Figs. 7 and 8) make it difficult to define intervals with consistent orientation. Furthermore, it is impossible to define surfaces between layers with consistent orientation. However, the change of bedding attitudes defines a surface between two adjacent intervals, and TrackDip provides the best constraints on specifying the depth of this surface (i.e. the depth location that optimizes the critical change in attitude). This surface is located between two successive measurement depths; therefore the precision on its depth depends on the local density of measurements. For example, the location of rotation 2 (541 mbsf; Fig. 7) can be between the m5.45 and m5.47 seismic boundaries, because no bedding surfaces were measured on the acoustic borehole televiewer in this interval. More precisely, rotation 2 cannot be better located than between the highest and lowest measurements, at 533.3 and 547.5 mbsf, respectively (Fig. 7). On the contrary, rotation 3 (416.12 mbsf) is well located between two close measurements at 415.29 and 416.14 mbsf (Fig. 8).

The changes in bedding attitudes do not appear to correlate to lithostratigraphic units or subunit boundaries. In the studied interval, almost all lithostratigraphic boundaries correspond to an uphole decrease in gamma ray value, with the only exception at the VB-VC boundary. While TrackDip rotation 3 (416.12 mbsf) may be the only one to match a lithostratigraphic boundary (IIIB-IIIC; Figs. 7 and 8), many others fit gamma ray local maxima (2, 12, 13, 24, 25) or minima (5, 6, 11) (Figs. 7 and 8). Because of the low measurement density at 500 mbsf, rotation 5 (491 mbsf) may also fit the gamma ray maximum at 498 mbsf. Similarly, rotation 13 (431 mbsf) may also correspond to the 430 mbsf gamma ray minimum.

Unlike lithostratigraphic boundaries, several seismic boundaries fit TrackDip rotations: rotation 3 (416 mbsf) corresponds to seismic surface m5.33, 5 (491 mbsf) corresponds to m5.35, and 2 (541 mbsf) corresponds to m5.45 or m5.47. Furthermore, there is a remarkable change of the trends of large-scale rotations above (north-south-trending 3-5) and below (east-west trending 6, 2, 7, and 1) the m5.4 seismic boundary at 512 mbsf (Fig. 7).

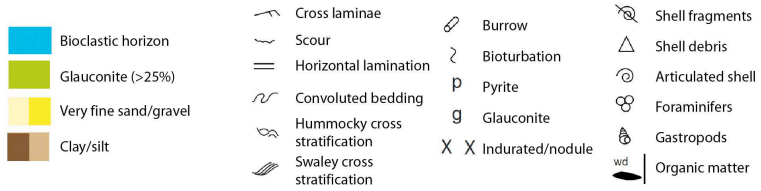

Figure 7 (continued): Lithostratigraphy, gamma ray log, bedding attitudes (dip and dip direction), and TrackDip (Basile et al., 2009) analysis in the investigated interval (mbsf-meters below seafloor). Blue dotted horizontal lines indicate lithostratigraphic boundaries; green horizontal lines indicate sequence boundaries from seismic lines. At the bottom of the azimuth and dip columns, the histograms show the prefered dip directions (black) and dips (grey) (118 measurements, maximum dip direction peak for 18 values, 25 for dips, same horizontal scales as the azimuth and dip plots). In the TrackDip column, red arrows represent the selected rotations as a function of depth and window size (cf. Fig. 5 for more details). Each rotation is computed between the mean orientations of strata in an upper and lower window (orange brackets above and below the red arrows). The rotations have to be tracked at least partly for window sizes with more than 7 measurements (right side of the dark green line) to be retained. The red arrows indicate the dip direction of the lower strata when the upper strata are set to horizontal. Their length is proportional to the rotation angle, and they are perpendicular to the rotation axis (cf. Fig. 5). The rotations are labelled (red numbers 1-25) from the wide windows to the thin ones. Stereonets (Wulf canvas, lower hemisphere) show the rotations 1-7. For each rotation, open black boxes are data from the upper interval, and filled black boxes are data from the lower interval. For rotation 1, black crosses are from the middle interval. The same red symbols represent the mean orientations for each interval. Great circles and rotations axis (stars) are computed from the mean orientations; red arrows indicate the rotation as in the TrackDip column.

DISCUSSION

Characteristic Scales for Changes of Bedding Attitudes

TrackDip identifies a rotation based on the change in mean bedding orientation across a given surface evaluated at different vertical scales of investigation, therefore for several data sets. This does not mean that the bedding attitudes do not vary within these investigated windows, rather that the mean orientation variation above and below the surface is stable. This is similar to what can be seen on a seismic line: inside a single seismic unit (defined by concordant reflectors), dips can vary from place to place; but the boundaries of each unit are defined by similar angular relationships (i.e., onlaps, downlaps…).

For a given rotation, TrackDip identifies the best window size (i.e. the characteristic scale for this rotation) from the highest rotation angle. Among the various scales where this rotation is observed (tracks in Figs. 5, 7 and 8), the largest scales indicate more progressive changes, while the smallest scales indicate more localized changes, that can be interpreted as an unconformity when each investigated window contains only one measurement (Basile et al., 2009). For example, rotation 19 (552 mbsf, Fig. 7) can be tracked over 11 scales from 4.75-0.475-m-thick windows. The best window size in this case is the smallest, indicating a localized rotation between two consecutive beds. On the contrary, the best window size for rotation 25 (426 mbsf, Fig. 8) is 0.95 m, for investigated windows ranging from 1.19 to 0.15 m over 10 different scales. In this case the best rotation almost corresponds to the largest window size, and should be interpreted as a progressive change between two sets of beds.

In this study, most tracked rotations are selected for their larger window scales. This is especially the case for rotations detected for window sizes thicker than 15 m that taken together covers approximately the entire studied interval. Most of these large-scale windows contain several measurements, indicating progressive changes of orientations instead of unconformable surfaces. Moreover, some rotations (such as 1 across the interval 548-660 mbsf in Fig. 7, or 21 between 414.4-419 mbsf in Fig. 8) occur over several successive depth intervals, indicating a progressive tilt. Rotation 1 results from not one but two successive rotations with similar trends and rotation way: a first rotation of 6.1° (N79° trend) occurs between the 547-586 and 586-623 mbsf intervals, and a second one of 5.8° (N86° trend) occurs between the 586-623 and 523-661 mbsf intervals. This indicates a progressive rotation of 11.9° over the 547-661 mbsf interval. This progressive tilt is in

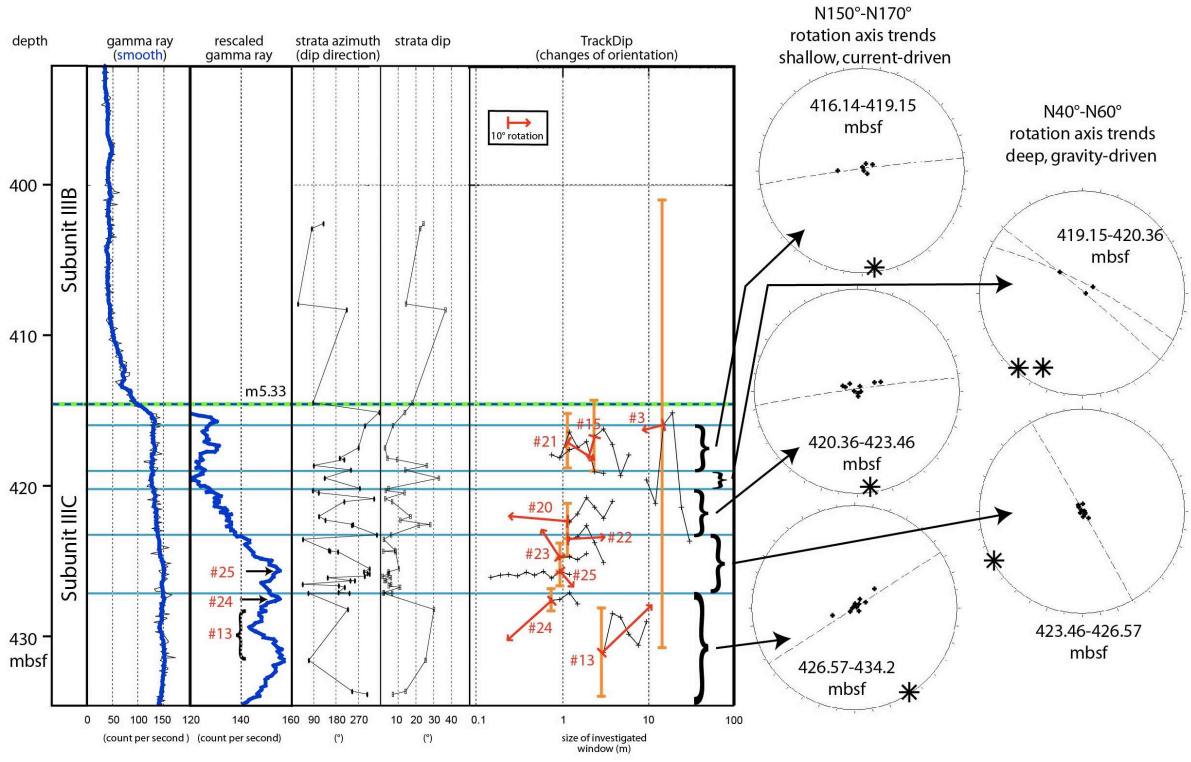

Figure 8: Enlarged view of the high-resolution interval [396-426 m below seafloor (mbsf), extended to 435 mbsf]. Same legend as in Figure 7; Wulf canvas, lower hemisphere. Crosses are poles of strata, stars are rotation axes.

good agreement with the offshore depositional environment and the absence of erosional surfaces observed in cores (Expedition 313 Scientists, 2010c). This does not exclude sudden rotations between successive bedding measurements, such as rotations 19 or 8 (552 and 648 mbsf, Fig. 7). However, because these rotations do not appear for the larger scales where rotations 7 and 1 occur at the same depth, they may be interpreted as local sedimentary structures (at scales of 1 to several meters) such as oblique or cross-bedding, rather than as unconformities between units that are thicker than tens of meters.

Interpretation of Rotation Axis Trends

Because changes of bedding attitudes are related to scales thicker than 15 meters, it is not possible to infer their origin from core (i.e. meter scale) observations. However, the scale is similar to the vertical resolution of available seismic lines and comparison of TrackDip analyses with these profiles provides additional insight into trends deduced from BHTV measurements.

First, seismic lines show a consistent southeast-dipping slope (N145° on average) in the studied interval, with the steepest surfaces within foreset reflectors immediately above seismic surface m5.4 (Fig. 3 and Table 1). We interpret rotation axes with trends sub-perpendicular to this dip direction (northeast-southwest trends) as related to gravity-driven processes, either during sedimentation, or after sedimentation in sliding and/or gliding processes, which can likely produce the steep dips (>20°) observed on cores and borehole images.

Second, TrackDip analysis shows consistent trends at a large scale (>10 m) above (north-south trending) and below (east-west trending) seismic surface m5.4. On the seismic lines (Fig. 3), this surface divides the overlying prograding section from the underlying aggrading section. This change is also related to a change in the strike direction of elongated depocenters, with depocenters striking N20-N35° for the overlying sequences m5.3 (above the investigated interval), m5.4 (drill site located above the depocenter) and m5.45 (depocenter northwest of the borehole), and N70° for sequences m5.6 and m5.7 (depocenters west of the borehole) (Monteverde et al., 2008, Figs. 5 and 6 therein). This may be related to changes in the location of the siliciclastic inputs in the marine basin and to the detailed shape of deltaic sedimentary bodies. Even if TrackDip trends differ from the depocenter elongation, the synchronous change suggests that large-scale rotation axes are also controlled by the geometry of the sedimentary bodies.

Sedimentary processes are also expected to control rotation-axis trends. This is especially the case for sedimentary accumulation driven by currents, which results in non-parallel laminae or beds. These rotations should have characteristic scales similar to the thickness of sedimentary structures, and would be observed only at small (decimeter to meter) scales. However, rotations should also be affected by large scale changes in the sedimentary processes, for example when the depositional environment changes from a shoreface dominated by waves to an offshore dominated by along shelf currents (Monteverde et al., 2008).

Correlation of Surfaces

One goal of this work was to determine if changes in orientation can be tied to stratigraphic surfaces defined by features in seismic lines (seismic surfaces), or by lithologies (boundaries between lithostratigraphic units). It appears that at least some seismic surfaces (m5.33, m5.35, m5.45 or m5.47, and indirectly m5.4) correlate with changes in bedding attitude. However, it is clear from the steep beds observed in cores and borehole images that these changes are not representative of the subtle dip variations on the seismic lines. With the available data, it is not possible to determine if the other seismic surfaces are not associated with changes of bedding attitude, or if the lack of measurement precludes their identification.

When compared to lithostratigraphic boundaries, there is almost no correlation with changes of orientation. However, many changes are correlated with maxima or minima in the gamma ray record. In the studied interval these maxima and minima can not be directly interpreted as variations in water depth at the time of deposition (e.g., with a maximum water depth corresponding to a gamma ray peak inferring a local clay maximum), because these variations in gamma ray value are also controlled by the glauconitic content (identified by Th/K ratio) and/or by the uranium content associated with organic matter (Expedition 313 Scientists, 2010c). However, these compositional changes should be associated with modifications of the sedimentary processes, and are consequently recorded as changes of orientations.

Parasequence Identification?

The bed-to-bed analysis can be interpreted as revealing small-scale sequences or parasequences in the 416-435 mbsf interval. Several successive intervals present consistent rotations axes, which alternate between two main trends. The 423.5-426.6 mbsf and 419.1-420.4 mbsf intervals present consistent N40°-N70°-trending rotation axes that can be related to gravity-driven processes, and interpreted as representative of a relatively deep sedimentary environment such as the foreset slope. The other intervals (416.1-419.1; 420.4-423.5; 426.6-435) also present consistent rotation axes, but these are trending N150° to N170°. The sudden change of rotation axis observed at 423.5 mbsf can be related to a sequence boundary, and the north-south-

trending rotation axis above 424 mbsf can be interpreted as reflecting a shallower deposition environment, influenced by currents. In this scheme, the upward changes from north-south to N45°-trends (419-424 mbsf) can be interpreted as an upward deepening of the sedimentary environment, before a shallowing (416-419 mbsf) with other north-south-trending rotation axis (Fig. 8). In this interpretation, the N45°-trending rotation axis at 419.5 mbsf corresponds to a maximum flooding surface.

CONCLUSIONS

As expected from examination of seismic lines and cores, there is no direct correlation in the studied interval at Site M28 between the orientations of sedimentary surfaces at a scale of tens of meter (seismic profiles) and a sub-meter scale (cores or borehole images). At a small scale, bedding attitudes present huge variations in both dip and dip direction that are not observed at the seismic scale. Furthermore, lithologic or seismic stratigraphic units cannot be related to a given and stable orientation of sedimentary strata.

However, change of orientation, defined as a rotation between two successive intervals, makes it possible to study the bedding attitudes at various scales, and appears to provide a tool consistent with the other data sets. TrackDip analysis was shown to be able to identify very small changes of orientations (2° rotation) in a scattered signal. At Site M28, the depths of the orientation changes fit very well with four of the eight seismic sequence boundaries, with characteristic scales similar to the thicknesses of the sedimentary sequences. Furthermore, the upward change from aggradational sequences to progradational sequences is also well recorded as a change in the large-scale rotation axis. It seems that seismic lines and the changes of strata orientations correlate to recorded large-scale changes of both physical properties of the sediments (that controls the seismic reflections) and bedding attitudes.

At a small scale, the orientation changes relate to sedimentary processes such as gravity-driven downslope sediment transport within foresets. However most changes do not correlate to the downslope direction observed on the seismic lines, indicating that many processes influencing the geometry of sedimentary bodies can not be truly understood in a single dip section, and that coast-parallel currents should be an important mechanism affecting bedding attitude.

The depths of change in orientation derived from TrackDip do not fit very well with lithostratigraphic units boundaries. However, they frequently correlate with maxima and minima in the gamma ray signal, suggesting the strong influence of changes in sedimentary processes rather of changes in lithology.

The use of bedding attitudes, as other methods, depends on the quality and resolution of the data, which were quite poor in this study, because, Site M28 drilled in a setting with enormous challenges to perfect core recovery. To achieve higher quality and more data values to assess, a study of bedding attitudes might be more readily applied to fully lithified sediments where bedding features are better preserved and easier to identify and measure.

ACKNOWLEDGEMENTS

This research used data provided by the Integrated Ocean Drilling Program (IODP) and International Continental Scientific Drilling Program (ICDP). We thank all the participants of IODP Leg 313 including crew, drillers, loggers, technical and administrative staff from ECORD (European Consortium for Ocean Drilling Research) and MARUM (Zentrum für Marine Umweltwissenschaften), and the entire scientific party offshore and onshore. We also thank two anonymous reviewers for their helpful comments, and Gregory Mountain for his editorial assistance. This work has been funded by CNRS-INSU (Centre National de la Recherche Scientifique-Institut National des Sciences de l'Univers).

REFERENCES CITED

Basile, C., Pecher, A., Corazzi, M., Odonne, F., Maillard, A., Debroas, E.J., and Callot, P., 2009, TrackDip: a multi-scale processing of dipmeter data – Method, tests, and field example for 3D description of gravity-driven deformations in the Eocene foreland basin of Ainsa, Spain: Marine and Petroleum Geology, v. 26, p. 738-751, 2009, doi: 10.1016/j.marpetgeo.2008.03.013.

Bellotti, P., Chiocci, F.L., Milli, S., Tortora, P., and Valeri, P., 1994, Sequence stratigraphy and depositional setting of the Tiber Delta; integration of high-resolution seismics, well logs, and archeological data: Journal of Sedimentary Research, v. 64, p. 416-432, doi:10.1306/D4267FDC-2B26-11D7-8648000102C1865D.

Donselaar, M.E. and Schmidt, J.M., 2005, Integration of outcrop and borehole image logs for high-resolution facies interpretation: example from a fluvial fan in the Ebro Basin, Spain: Sedimentology, v. 52, p. 1021–1042, doi:10.1111/j.1365-3091.2005.00737.x.

Donselaar, M.E., and Schmidt, J.M., 2010, The application of borehole image logs to fluvial facies interpretation, *in* Poppelreiter M., et al.,

eds., Dipmeter and borehole image log technology: American Association of Petroleum Geologists Memoir 92, p. 145–166.

Expedition 313 Scientists, 2010a, Expedition 313 summary, *in* Mountain, G., et al., Proc. IODP, 313: Tokyo (Integrated Ocean Drilling Program Management International, Inc.), doi:10.2204/iodp.proc.313.101.2010.

Expedition 313 Scientists, 2010b, Methods, *in* Mountain, G., et al., Proc. IODP, 313: Tokyo (Integrated Ocean Drilling Program Management International, Inc.), doi:10.2204/iodp.proc.313.102.2010.

Expedition 313 Scientists, 2010c, Site M0028, *in* Mountain, G., et al., Proc. IODP, 313: Tokyo (Integrated Ocean Drilling Program Management International, Inc.), doi:10.2204/iodp.proc.313.104.2010.

Fulthorpe, C.S., Mountain, G.S., and Miller, K.G., 1996, Mapping Neogene depositional geometries, New Jersey continental slope, Leg 150 drilling area, *in* Mountain, G.S., et al., eds.: Proceedings of the Ocean Drilling Program, Scientific results, v. 150: College Station, Texas, Ocean Drilling Program, p. 269-281, doi:10.2973/odp.proc.sr.150.021.1996.

Greenlee, S.M., and Moore, T.C., 1988, Recognition and interpretation of depositional sequences and calculation of sea level changes from stratigraphic data-Offshore New Jersey and Alabama Tertiary, *in* Wilgus, C.K., et al., eds, Sea-Level changes: Society of Economic Paleontologists and Mineralogists Special Publication 42, p. 329-353, doi:10.2110/pec.88.01.0329.

Greenlee, S.M., Devlin, W.J., Miller, K.G., Mountain, G.S., and Flemings P.B., 1992, Integrated sequence stratigraphy of Neogene deposits, New Jersey continental shelf and slope: Comparison with the Exxon model: Geological Society of America Bulletin, v. 104, p. 1403-1411, doi:10.1130/0016-7606(1992)104<1403:ISSOND>2.3.CO;2.

Haggas, S.L., Brewer, T.S., Harvey, P.K., and Iturrino, G.I., 2001, Relocating and orientating cores by the integration of electrical and optical images: A case study from Ocean Drilling Program Hole 735B: Journal of the Geological Society of London, v. 158, p. 615-623, doi:10.1144/jgs.158.4.615.

Hathaway, J.C., Schlee, J.S., Poag, C.W., Valentine, P.C., Week, W.G.A., Bothner, M.H., Kohout, F.A., Manheim, F.T., Schoen, R., Miller, R.E., and Schultz, D.M., 1976, AMCOR - Preliminary report of the 1976 Atlantic Margin Coring Project of the US Geological Survey, US Geological Survey Open File Report 76-844, 207 p.

Inwood, J., Brewer, T., Braaksma, H., and Pezard, P., 2008, Integration of core, logging and drilling data in modern reefal carbonates to improve core location and recovery estimates (IODP Expedition 310): Journal of the Geological Society, v. 165, p. 585-596, doi:10.1144/0016-76492007-041.

Luthi, S.M., 1990, Sedimentary structures of clastic rocks identified from electrical borehole images, *in* Hurst, A., et al., eds., Geological applications of wireline logs, Geological Society of London Special Publications, v. 48, p. 3-10, doi:10.1144/GSL.SP.1990.048.01.02.

Luthi, S.M., and Banavar, J.R., 1988, Application of borehole images to three-dimensional geometric modeling of eolian sandstone reservoirs, Permian Rotliegende, North Sea: American Association Petroleum Geologist Bulletin, v. 72, p. 1074-1089.

Luthi, S.M., Hodgson, D.M., Geel, C.R., Flint, S.S., Goedbloed, J.W., Drinkwater, N.J., and Johannessen, E.P., 2006, Contribution of research borehole data to modeling fine-grained turbidite reservoir analogues, Permian Tanqua-Karoo basin-floor fans (South Africa): Petroleum Geoscience, v. 12, p. 175-190, doi:10.1144/1354-079305-693.

MacLeod, C.J., Parson, L.M., and Sager, W.W., 1994, Reorientation of cores using the Formation Microscanner and Borehole Televiewer: application to structural and paleomagnetic studies with the Ocean Drilling Program, *in* Hawkins, J., et al., Proceedings of the Ocean Drilling Program, Scientific Results, v. 135 : College Station, Texas, Ocean Drilling Program, p. 301-311, doi:10.2973/odp.proc.sr.135.160.1994.

Monteverde, D.H., Mountain, G.S., and Miller, K.G., 2008, Early Miocene sequence development across the New Jersey margin: Basin Research, v. 20, p. 249-267, doi:10.1111/j.1365-2117.2008.00351.x.

Mountain, G.S., Miller, K.G., and Blum, P., 1994, Proceedings of the Ocean Drilling Program, Initial reports, v. 150 : College Station, Texas, Ocean Drilling Program, 885 p., doi:10.2973/odp.proc.ir.150.1994.

Mountain, G., Proust, J.-N., McInroy, D., Cotterill, C., and the Expedition 313 Scientists, 2010, Proc. IODP, 313: Tokyo (Integrated Ocean Drilling Program Management International, Inc.), doi:10.2204/iodp.proc.313.2010.

Parkinson, D.N., Dixon, R.J., and Jolley, E.J., 1999, Contributions of acoustic imaging to the development of the Bruce Field, northern North Sea, *in* Lovell, M.A., et al., eds., Borehole imaging: applications and case histories: Geological Society, London, Special Publications, v. 159, p. 259-270, doi:10.1144/GSL.SP.1999.159.01.14.

Prensky, S.E., 1999, Advances in borehole imaging technology and applications, *in* Lovell, et al.,

eds., Borehole imaging: applications and case histories: Geological Society, London, Special Publications, v. 159, p. 1-43, doi:10.1144/GSL.SP.1999.159.01.01.

Prosser, J., Buck, S., Saddler, S., and Hilton, V., 1999, Methodologies for multi-well sequence analysis using borehole image and dipmeter data, *in* Lovell, M.A., et al., eds., Borehole imaging: applications and case histories: Geological Society, London, Special Publications, v. 159, p. 91-121, doi:10.1144/GSL.SP.1999.159.01.05.

Puga-Bernabéu, A., and Betzler, C., 2008, Cyclicity in Pleistocene upper-slope cool-water carbonates: Unraveling sedimentary dynamics in deep-water sediments, Great Australian Bight, ODP Leg 182, Site 1131A : Sedimentary Geology, v. 205, p. 40-52, doi:10.1016/j.sedgeo.2008.01.008.

Serra, O., 1989, Formation microscanner image interpretation: Houston, Schlumberger Educational Services SMP-7028, 117 p.

Steckler, M.S., Mountain, G.S., Miller, K.G., and Christie-Blick, N., 1999. Reconstruction of Tertiary progradation and clinoform development on the New Jersey passive margin by 2-D backstripping: Marine Geology, v. 154, p. 399-420, doi:10.1016/S0025-3227(98)00126-1.

Vail, P.R., Mitchum, R.M. Jr, Todd, R.G., Widmier, J.M., Thompson, S. III, Sangree, J.B., Bubb, J.N., and Hatlelid, W.G., 1977, Seismic stratigraphy and global changes of sea level, *in* Payton C.E., ed., Seismic stratigraphy applications to hydrocarbon exploration: American Association Petroleum Geologists Memoir, v. 26, p. 49-212.

Van Wagoner, J.C., Mitchum, R.M., Campion, K.M., and Rahmanian, V.D., 1990, Siliciclastic sequence stratigraphy in well logs, cores, and outcrop: concepts for high-resolution correlation of time and facies, American Association of Petroleum Geologists Methods in Exploration Series, v. 7, 55 p.

Williams, J.H., and Johnson, C.D., 2004, Acoustic and optical borehole-wall imaging for fractured-rock aquifer studies: Journal of Applied Geophysics, v. 55, p. 151-159, doi:10.1016/j.jappgeo.2003.06.009.

Yamada, Y., McNeill, L., Casey Moore, J., and Nakamura, Y., 2011, Structural styles across the Nankai accretionary prism revealed from LWD borehole images and their correlation with seismic profile and core data: results from NanTroSEIZE Stage 1 expeditions: Geochemistry Geophysics Geosystems, v. 12, 7 p., Q0AD15, doi:10.1029/2010GC003365.